In silico study of the ageing effect upon aortic valves

Anna Maria Tango[1], Andrea Ducci[1], Gaetano Burriesci[1,2]

[1]UCL Mechanical Engineering, University College London, Torrington Place, London, WC1E 7JE, UK

[2]Bioengineering Unit, Ri.MED Foundation, Via Bandiera 11, 90133, Palermo, Italy

Abstract

A fluid-structure interaction (FSI) numerical model of the aortic valve was used to simulate and compare young and physiological aged operating conditions. The effect of normal ageing was considered by introducing alterations typically associated with senility: namely mild stiffening of the tissues and progressive dilation of the aortic chamber. The aim of this study is to provide a haemodynamic baseline which allows to assess the typical physiological variations associated with advancing age. Results were analysed in terms of leaflets kinematics, flow dynamics, pressure and valve performance parameters. The study indicates that the normal changes occurring with ageing, such as stiffening and progressive aortic root dilation, can result in substantial alterations in the haemodynamics and mechanical efficiency of the aortic valve. In particular, mild tissue stiffening and aortic root dilation reduce the valve efficiency over the cardiac cycle. The concomitant presence of both phenomena can lead to some mitigation of the impairment. The observed changes, which can be associated with normal and healthy ageing, need to be taken into consideration when evaluating the real pathological contribution of aortic valve diseases occurring in aged patients.

Keywords: Fluid–structure-interaction (FSI), Heart valve dynamics, Haemodynamics, Ageing.

Introduction

Ageing is often associated with degenerative pathological conditions of the aortic valve and root such as senile aortic valve calcification (Tamburino,C.,Ussia, 2012) or aneurysm, which result from the presence of an over-dilated aorta (Kirali and Günay, 2017). These pathologies have been the object of extensive studies to identify their effect on the hydrodynamic function (Amindari et al., 2017; Barannyk and Oshkai, 2015; Marom et al., 2013; Querzoli et al., 2014; Toninato et al., 2016; Yoganathan, 1988). However, the normal ageing process itself, even in healthy conditions, involves anatomical variations in the human aortic root (Mao et al., 2008; Roman et al., 1987; Sahasakul et al., 1988; Sugawara et al., 2008; Virmani et al., 1991; Vriz et al., 2014) which are not associated with diseased conditions and can therefore be considered entirely physiological. In fact, normal ageing leads to degenerative changes upon the tissues in the aortic root and valve, which result from a complex interplay between the haemodynamics and biological processes (Bäck et al., 2013). In particular, from the age of 40, the aortic root progressively expands its diameter at the sino-tubular junction (STJ) and sinuses region (Virmani et al., 1991; Vriz et al., 2014) by about 1 mm per decade (Craiem et al., 2012; Martin et al., 2013), whilst vascular tissues stiffen (Sugawara et al., 2008) and remodel (Guala et al., 2015) and aortic valve cusps (Sahasakul et al., 1988) thicken, especially after the fifth decade. The enlargement of the STJ region occurring with advancing age is not associated with an equivalent dilation of the annulus, causing an increasing mismatch between the dimensions of these two regions (Virmani et al., 1991; Vriz et al., 2014), which in the healthy young condition have similar size (Thubrikar, 1990). This process is typically associated with arteriosclerosis, the most widespread age-associated change in the vascular system, which in its general form consists in the progressive thickening and stiffening of the arterial walls. Its potential effect on the performance of the aortic valve is acknowledged by the international regulation for the assessment of cardiac valve prostheses (International Standard ISO 5840), which requests that stentless valves are tested in chambers of two specified values of compliance. Similarly, valve cusps thicken with ageing in all regions, about doubling their average thickness when patients progress from 20 to 75 year old (Sahasakul et al., 1988).

All these variations may potentially lead to functional alterations. Therefore, in order to correctly interpret pathological conditions and their isolated impact on the aortic valve, it is

essential to understand if and how normal ageing is expected to modify the operating mechanisms and the efficiency of these components.

This study attempts to provide a haemodynamic baseline for the physiological changes due to ageing, analysing independently the potential contribution of the main age related factors.

Materials and Methods

In order to simulate the valve behaviour, both the leaflets mechanical response and their motion due to the load exerted by the surrounding fluid need to be modelled in the numerical analysis (Sacks et al., 2009). Hence, fluid-structure interaction (FSI) is the most suitable and comprehensive computational approach to accurately simulate the valve dynamics (Carmody et al., 2006; Marom, 2015; Sturla et al., 2013).

The analyses were performed using the explicit finite element software LS-DYNA (LSTC, Livermore, CA, USA) on an Intel Core i7 3.4 GHz workstation.

The models include the aortic root and valve, immersed in a fluid domain. Both the structure and fluid were meshed using ICEM 17.0 (ANSYS, Inc., Canonsburg, PA, USA) and then exported to LS-DYNA. An arbitrary Lagrangian–Eulerian (ALE) algorithm was used to implement the coupling between the structural and fluid elements. This, given the boundary conditions, remaps the solution from the distorted to the undistorted mesh but, unlike a rezoning, the mesh topology is kept fixed (Hallquist, 2006; M. Souli, A. Ouahsine, 2017).

Results were analysed using both LS-PrePost 4.3 and Paraview 5.4.1 post-processing software.

Fluid domain

The fluid domain was discretised into a grid of 113,520 8-noded hexahedral Eulerian elements with a characteristic dimension of 1 mm, selected based on a grid convergence study (Tango et al., 2018).

Geometry and mesh for the fluid domain were left unaltered in all models.

Blood was assumed to be Newtonian (Annio et al., 2019; Wei et al., 2018), isothermal and nearly incompressible, with a density of 1060 kg/m^3 and a dynamic viscosity of 4×10^{-3} Pa·s in all FSI analyses.

The aortic pressure waveform was applied at the outlet throughout the cardiac cycle. A uniformly distributed flow velocity corresponding to a cardiac output of 4 l/min was applied

at the ventricular inlet during the systolic phase. In order not to enforce a specific regurgitant flow during closing, in the diastolic phase the boundary condition at the ventricular inlet was substituted with a typical ventricular pressure waveform. Three cardiac cycles were simulated, as flow parameters were found to become repeatable from the 2nd cycle. The used boundary conditions are described in Figure 1 (c).

Structural domain

The aortic root and the valve leaflets structural domains were discretized into 9960 and 6564 4-noded Belytschko-Tsay shell elements (Hallquist, 2006), respectively. Uniformly distributed thicknesses of 0.5 and 3.0 mm were used for the aortic leaflets and root walls, respectively (Joda et al., 2016; Nobari et al., 2013; Sirois, 2014; Sturla et al., 2013). The obtained model is shown in Figure 1 (a).

Mesh, geometry and computational setup were all consistent with the validated numerical framework described in Tango *et al.* (Tango et al., 2018), where further details on the applied boundary conditions, mesh and adopted geometry can be found.

Young healthy model

The aortic root was modelled following the description of the young healthy human anatomy provided by Swanson and Clark (Swanson and Clark, 1974) in reference to an annulus equal to 25 mm, corresponding to an average young healthy adult (Thubrikar et al., 2005). This identifies an average diameter at the sino-tubular junction identical to that of the annulus. The idealised leaflet geometry provided by Thubrikar (Thubrikar, 1990) was used to model a healthy aortic valve with a corresponding annulus diameter equal to 25 mm.

Due to their highly nonlinear large deformation response[5], leaflets were approximated as isotropic non-linear hyperelastic (Figure 1 (d)), using an Ogden constitutive model (Zhang et al., 2007), as described in Tango *et al.* (Tango et al., 2018).

The aortic root wall was modelled with linear elastic material (Figure 1 (d)), with a Poisson's ration of 0.45 and Young's modulus of 0.92 MPa, modelling a high compliance aortic root (compliance C = 0.32 %/mmHg) (International Standard ISO 5840:2009).

Stiffened model

The alterations that ageing typically induces upon the flow dynamics were investigated. In particular, the contributions of stiffening/thickening of the tissues and dilation of the aortic root were investigated separately, in order to identify the implications related to each factor. As these age-related changes are typically correlated and concomitant, their combined effect was then analysed in the final model (Crawford and Roldan, 2001; Wilton and Jahangiri, 2006).

In order to mimic the age-related thickening of the valve cusps, the geometry and mesh description were left unaltered with respect to the young healthy configuration (see Figure 1(a)) whilst the thickness of the valve cusps was doubled from 0.5 to 1 mm, maintaining the same material model defined for the young healthy configuration (Seki and Fishbein, 2016).

To model aged conditions, the rigidity of the linear elastic material used for the young healthy aortic walls was adjusted, based on the recommendation from the international standard ISO 5840 for simulating patients with a low compliance aorta (compliance C = 0.09 %/mmHg) (International Standard ISO 5840:2009) therefore resulting in a Young's modulus value of 3.25 MPa.

Expanded models

The model of the expanded aortic root was realised by linearly scaling the aortic root along the axis from the annulus cross section, which was maintained at a diameter of 25 mm, up to the STJ level, which was expanded to reach a diameter of 29 mm (see Figure 1(b)). This level of expansion can be considered representative of patients over 65 (Craiem et al., 2012; Martin et al., 2013). This model was analysed with the same thickness and material properties defined in the young healthy and stiffened models, respectively, in order to analyse the effect of each factor and the combined presence of the stiffened leaflets and enlarged aortic chamber, which are often concomitant in the elderly (Figure 1(b)).

A summary of the features characterising each configuration is presented in Table 1.

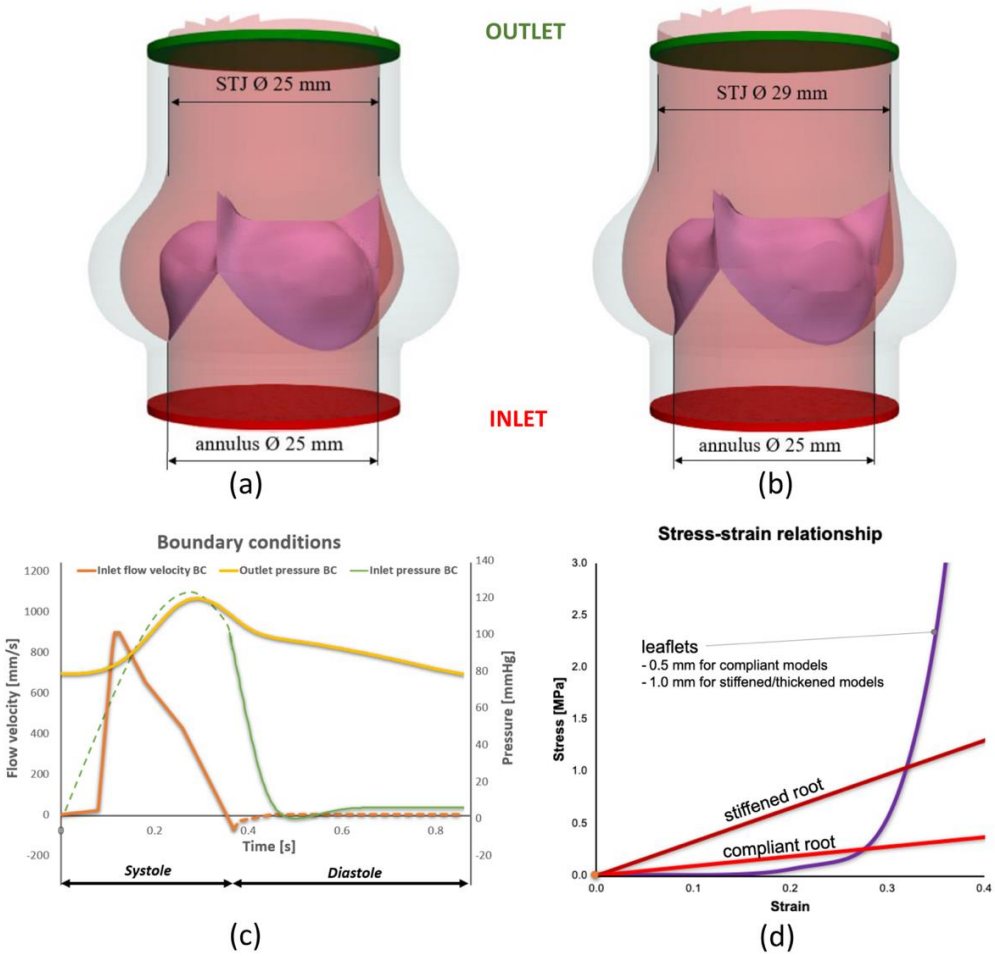

Figure 1. Geometry model used for the young healthy and stiffened valve (a), dilated root and stiffened valve in dilated root (b) configurations, applied boundary conditions (c) and mechanical response for young healthy and stiffened conditions for elastic and hyperelastic models (d).

Table 1. Parameters used for healthy and ageing configurations.

Configuration	Annulus diameter [mm]	STJ diameter [mm]	Root Young modulus [MPa]	Leaflets' thickness [mm]
Young healthy	25	25	0.92 *	0.5
Stiffened/Thickened tissues	25	25	3.25 *	1 [28]
Dilated root	25	29	3.25 *	0.5
Stiffened/Thickened tissues and dilated root	25	29	3.25 *	1 [28]

*The Young's modulus was estimated to match the two vessel compliances recommended in the international standard ISO 5840 (C=0.32%/mmHg and C=0.09%/mmHg)[12].

Results

The alterations of the aortic valve region typically associated with ageing, such as the mild stiffening/thickening of the tissues and the progressive aortic root dilation (Crawford and Roldan, 2001; Wilton and Jahangiri, 2006), were examined by comparing the data obtained for the aged configurations with those of a young healthy root. In particular, results were analysed in terms of leaflets kinematics, flow dynamics, pressure and valve hydrodynamic performance.

The analysis of flow and pressure measurements was performed by extracting the flow velocity maps and vectors in a slice bisecting one of the sinuses, and in a transversal plane at the level of the maximum diameter of the Sinuses of Valsalva.

Figure 2 shows the time instants of the cardiac cycle were the results were analysed: systolic peak (A), end of systole (B), early diastolic phase (C), full closure (D).

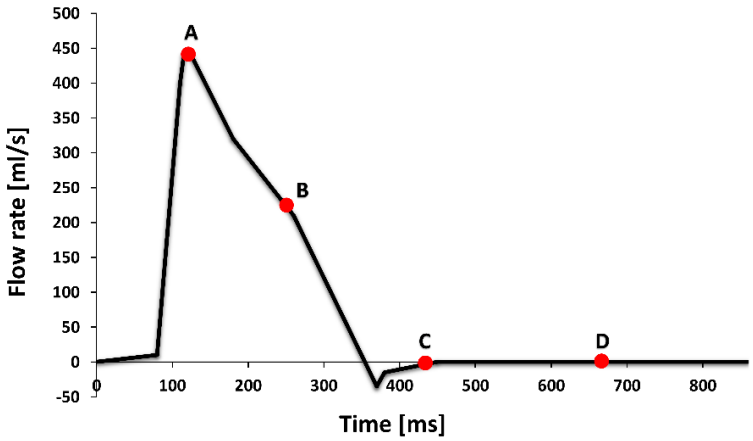

Figure 2. Time instants used for the analysis of the aortic valve hemodynamic.

Valve kinematics: valve opening (VOT), valve closure (VCT) and ejection time (ET)

The valve kinematics was studied by tracking the radial position of the upper middle node of one leaflet throughout the cardiac cycle.

Three main phases can be identified when characterising the leaflets motion: opening, closing (normally slower than the opening) and closed phases (Wendt et al., 2015). In agreement with the international standard ISO 5840(International Standard ISO 5840:2009), the valve opening and closing time characteristics were used to compare the valve kinematics.

Hence, the valve opening time (VOT) was defined as the time between initiation of leaflets opening and full valve opening (t_1 - t_2 in Figure 4 and 4), where the full valve opening corresponds to the instant where the leaflets have completed their reversal of curvature, to take a stable open configuration (this does not correspond to the time when the leaflets experience their maximum radial displacement, which is related with the expansion produced by the peak of transvalvular pressure, acting on the already open leaflets). Similarly, the valve closure time (VCT) was defined as the time between initiation of valve closure and full valve closure (t_3 - t_4 in Figure 4 and 4), with the full valve closure corresponding to the instant when the leaflets curvature has stabilized in closed configuration. The ejection time (ET) was measured as the total time between initiation of valve opening and complete valve closure (t_1 - t_4 in Figure 4 and 4)(Ranga et al., 2006).

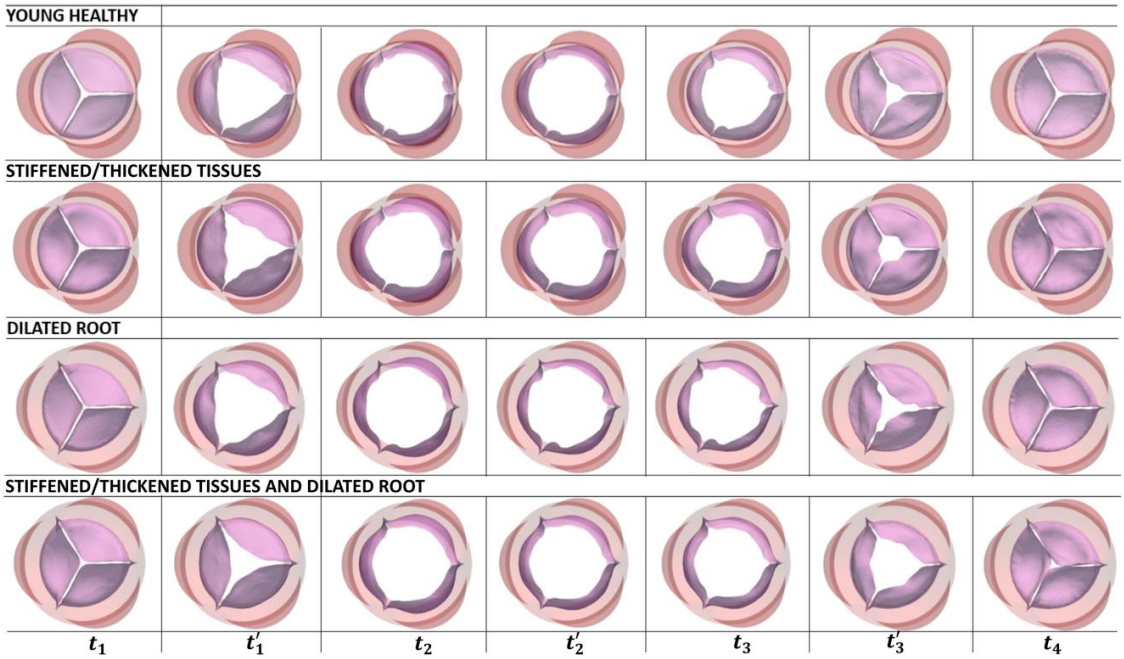

Figure 3.Valve top view for young healthy and aged configurations at the instants used for the calculation of the valvular kinematics parameters.

Figure 3 shows a visual comparison of the top view of the valve between young healthy and aged configurations during the most relevant time instants of the cardiac cycle, here used to

evaluate the valve kinematics. Models including stiffened/thickened tissues are characterised by slower opening (clearly shown in instant t_1') and present a narrower valve orifice when the valve is fully open (instant t_2). In terms of closure, the combination of stiff leaflets and dilated root slows down the valve closure (instant t_3').

The model with compliant tissues and dilated root walls presents a wider opening with a shape of the cusps more similar to that of the physiological case.

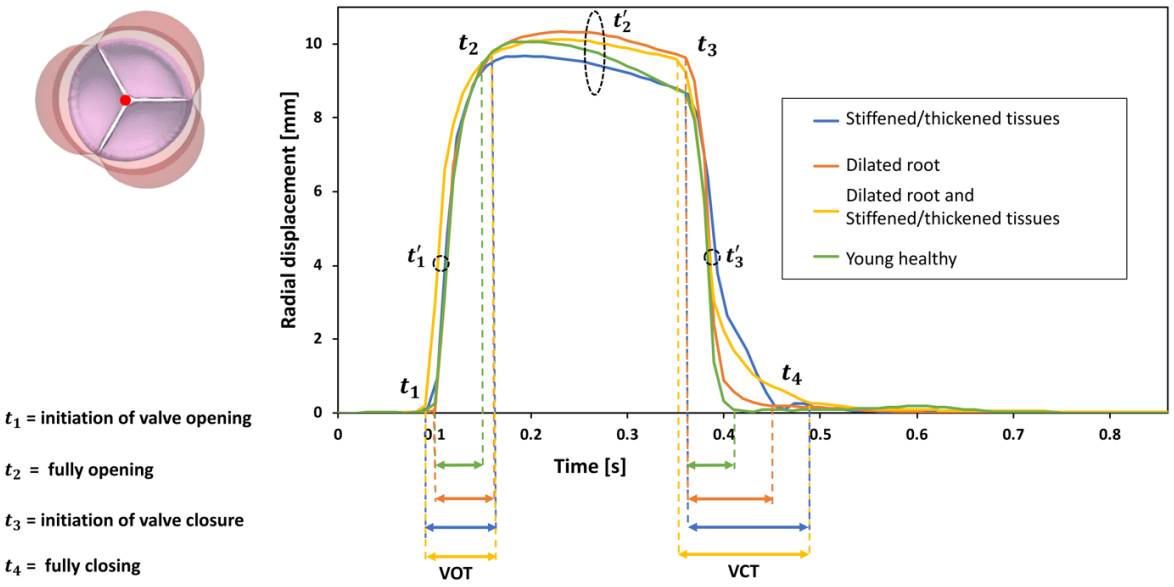

Figure 4. Graph used to compare the leaflets kinematics in young healthy (green), stiffened/thickened tissues (blue), dilated root (orange) and dilated root with stiffened/thickened tissues (yellow) configurations. The red point on the leaflet shows the location of the node where the displacement was tracked for all configurations.

Figure 4 shows that the young healthy configuration is characterised by the shortest opening and closing time. These times are consistent with *in vivo* (Leyh et al., 1999) and other numerical analyses (Nobari et al., 2012; Ranga et al., 2006) performed on healthy valves.

Stiffening of the tissues resulted in an earlier starting of the opening phase, and a substantially delayed complete closing, resulting in the longest VOT and VCTs. Interestingly, the opening of all altered configurations was completed at about the same instant, 10 ms later than for the young healthy model.

In terms of maximum radial displacement, the stiffened valve model presents the smallest displacement (9.68 mm), with a difference of -3.79% with respect to the young healthy analysis. In the expanded configurations, expectedly, a slightly wider leaflets displacement

was observed. In particular, the difference in percentage compared to young healthy conditions is +2.75 % for the model with the dilated root, and +0.57% for the model with both stiff cusps and dilated aortic root.

As shown in Table Table 2, the effect of alterations normally associated with ageing led to extensions in the VOT and VCT for all configurations. In particular, the model with a stiffened valve anchored in a dilated root, presents significantly extended opening and closure times since, in addition to a delayed closure, the leaflets displacement opening and closing initiation phases occur earlier than in the other pathological models.

Table 2. Valve opening, closure and ejection times for physiological and aged configurations.

Configuration	**VOT [ms]**	**VCT [ms]**	**ET [ms]**
Young healthy	50	50	310
Stiffened/thickened tissues	70	116	386
Dilated root	60	70	330
Stiffened/thickened tissues and dilated root	70	130	390

In terms of leaflets radial displacement, apart from the model replicating the stiffening of the valve, whose cusps' maximum extension is smaller by 4% than that measured in young healthy conditions (9.68 mm), both configurations including a dilated chamber produce a slightly wider displacement, respectively by 2.6 % for the model with an expanded root only (10.33 mm), and by 0.5% for the model including valve stiffening and root dilation (10.11 mm). This might be explained by the presence of longer leaflets free edges and larger sinuses.

Flow velocity

From the velocity maps (Figure 5) and velocity profiles (Figure 6) it can be observed how the jet at the systolic peak, which is well aligned with the axis of the aortic root for the models with no dilatation, becomes inclined when the diameter at the STJ becomes larger, due to the presence of larger vortices above the sinuses than above the commissures. These reduce the width of the systolic jet, which changes little compared to the young healthy case, even for the case where the tissue stiffness and thicknesses remain unchanged.

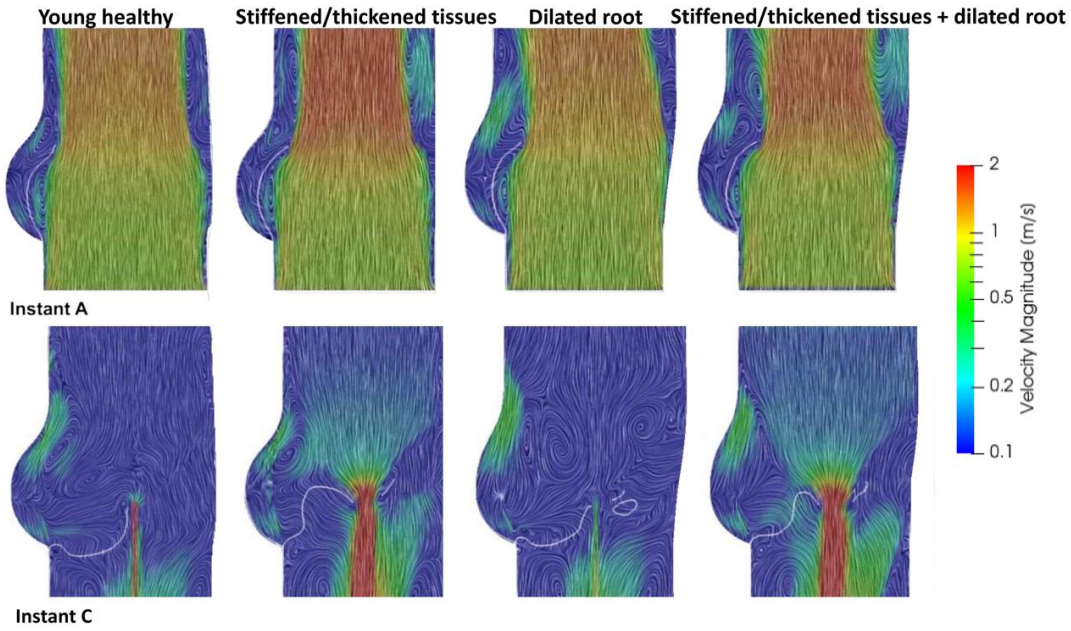

Figure 5.Velocity maps including leaflets opening (systolic peak) and closure profile (early diastole) obtained for the different models. The velocity streamlines are visualised using line integral convolution (LIC).

From Figure 5 it can be better appreciated how all the models including the stiffening/thickening of the tissues present a delayed closure and, therefore, a significant regurgitation through the valve orifice at early diastole.

It should be noted that the small reverse flow jet observed in all models at late diastole is a common artefact of the FSI methodology, which requires the inclusion of a small gap between the leaflets of the closed valve configuration in order for the valve to open (this was 0.1 mm in our models).

Thus, the analysis of the regurgitation levels is more significative for the closing regurgitant volume occurring during the valve closure than for the leakage occurring after closure, which is due to the methodology employed and is proportional to the length of the leaflets free edges (this is larger for the enlarged roots). The absence in our models of the nodulus of Arantius, the fibrous bulge at the centre of the leaflets' edge which contributes to achieve complete closure, may also justify the presence of the small regurgitant jet observed at the centre of the closed valve.

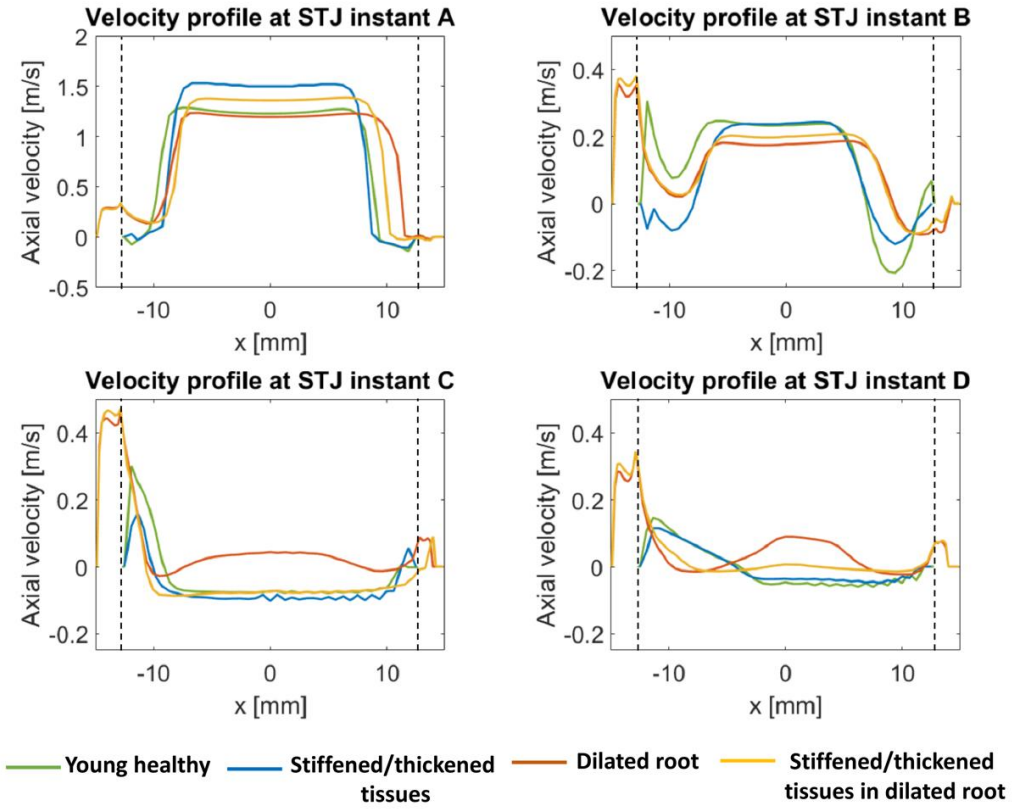

Figure 6. Comparison of the velocity profiles extracted at the STJ level for the healthy (green), stiffened valve (blue), dilated root (orange), stiffened valve in a dilated root (yellow) models. The dashed vertical lines indicate the walls of the 25 mm aortic root.

In terms of velocity profiles (Figure 6), in young healthy conditions the width of the fast jet flow at *instant A* is 16.16 mm therefore occupying the 64% of the STJ cross section. In terms of velocity peak magnitude (*instant A*), a value of 1.28 m/s was identified, consistently with other *in vivo* (Otto, 2000; Rossvoll et al., 1991), computational (Sturla et al., 2013) and experimental works (Zhang and Zhang, 2018).

The dilated root model is the one showing larger differences when compared to young healthy conditions. The maximum velocity of the slightly angulated forward flow at the systolic peak is 1.24 m/s, lower than the young model by 3.1%. The central flow width at the STJ is slightly wider than in the young healthy configuration (+5.19%). However, despite the presence of a wider aortic chamber at the STJ level for the jet to expand, the flow occupies just the 58% of the available space. Therefore, the root enlargement does not result in a proportionally enlarged central flow.

Narrower central jets are observed when stiffened/thickened tissues are modelled (-11.7% wide) and when the effect of stiffening/thickening is combined with the presence of a dilated

root (-5.63% wide), along with peak velocities of 1.53 m/s and 1.39 m/s (19.5% and 8.6% higher with respect to young healthy conditions, respectively).

Pressure maps, effective orifice area (EOA) and Transvalvular pressure gradient

Blood pressure distributions were examined across the same sagittal slice used to analyse the flow velocity at the times A, B, C, and D described in Figure 2. For further details, the reader is referred to Figures A9, A10, A11, A12 in the Appendix.

In order to verify the effect of the different configurations over the global parameters clinically used to assess the valve performance, the transvalvular pressure difference (ΔP) and effective orifice area (EOA) were computed. The latter, which corresponds to the cross section of the *vena contracta* at the valve exit, was estimated using equation (1), as recommended by the international standard ISO 5840 (International Standard ISO 5840:2015):

$$\mathrm{EOA} = \frac{\mathrm{q_{v_{RMS}}}}{51.6\sqrt{\frac{\Delta \mathrm{p}}{\rho}}}\ ; \qquad (1)$$

where $\mathrm{q_{v_{RMS}}}$ is the root mean square of the forward flow rate during the positive differential pressure period, expressed in ml/s; $\Delta \mathrm{p}$ is the mean pressure difference measured during the positive differential pressure period, expressed in mmHg; and ρ, is the density of the test fluid[9], expressed in g/cm^3.

A summary of the three performance parameters for all configurations investigated is provided in Table 3. As expected, the pressure overload caused by the leaflets stiffening is reflected on the transvalvular pressure measurement, which increases from 4.56 mmHg for the healthy young model to 7.68 mmHg, significantly worsening the valve performance.

Table 3. Transvalvular pressure drop, EOA and closing volume values for young healthy and aged configurations.

Configuration	Δp[mmHg]	EOA [cm^2]	Closing volume [ml]
Young healthy	4.56	2.94	11.83
Stiffened/Thickened tissues	7.68 (+68.4%)	2.26 (-23.1%)	17 (+43.7%)
Dilated root	3.95 (-13.3%)	3.16 (+7.4%)	14.62 (+23.58%)
Stiffened/Thickened tissues and dilated root	6.38 (+40%)	2.48 (-15.6%)	17.47 (+47.67%)

Interestingly, the positive effect of dilating the aortic root on the EOA is marginal. In fact, an enlargement of 35% in the cross section at the STJ (from 25 to 29 mm diameter) resulted into a marginal increase in the EOA (7.4 %) in the model where the tissue rigidity was not increased. It is also important to take into consideration that the cusps of the enlarged root model have a free edge which is 13.5% larger than the young healthy valve. In the models with stiffened/thickened tissues, the EOA, is reduced by 23.1% and by 15.6% with respect to young healthy conditions for the models with same geometry and dilated root, respectively (see Table Table 3). This is expectedly associated with an increase in Δp.

Pressure distributions

The pressure distribution in the sagittal plane gives an interesting insight into a mechanism previously described in Tango *et al.* (Tango et al., 2018), which contributes to enhancing the valve efficiency: the systolic jet at the valve exit produces a Venturi effect which determines a suction in the region between the open leaflets and the walls of the Sinuses of Valsalva, which increases the trans-leaflet opening pressure, promoting the leaflets expansion into the sinuses. This is observed in all models at the instant preceding the systolic peak, as shown in Figure 7.

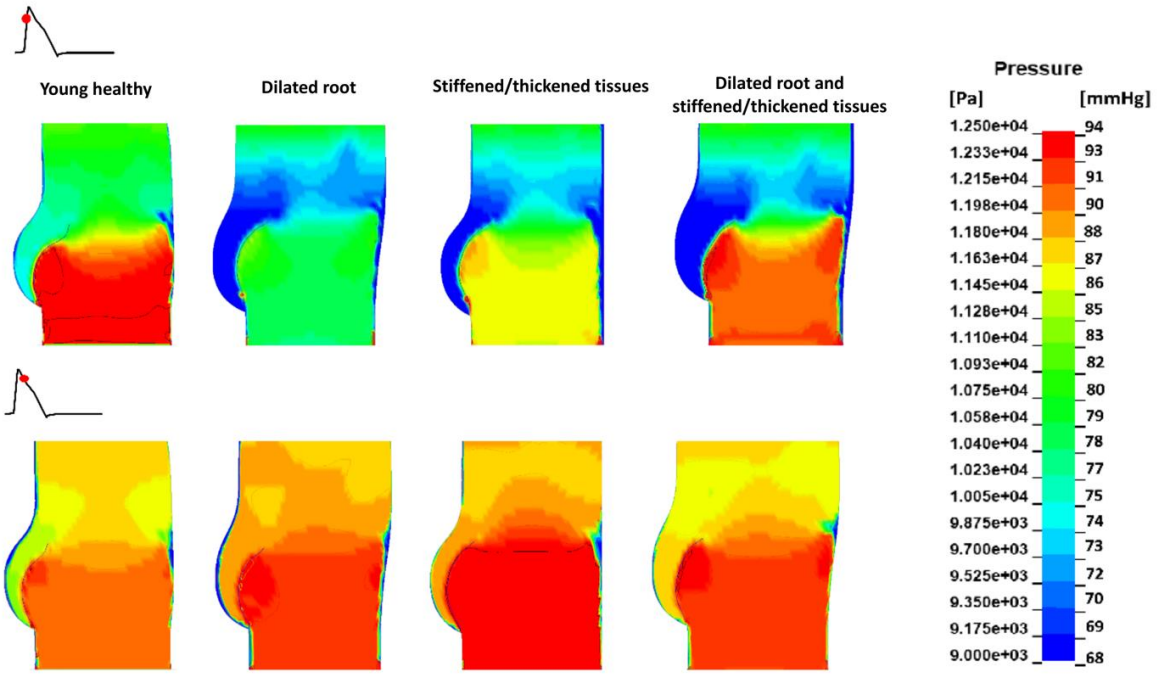

Figure 7. Pressure maps showing the maximum suction effect for young healthy and 'ageing' models at the instants preceding and following the systolic peak.

The highest suction, measured as the difference between the minimum pressure in the sinuses and the mean pressure above the STJ, is detected in aged models (the average suction for the all these models is consistently around 16 mmHg). This may be due to the presence of a larger chamber for the models including a dilated aorta, and to the leaflets thickening for the models reproducing mild leaflets stiffening. However, this effect fades very rapidly after the systolic peak. On the contrary, for the young healthy case the peak during suction is smaller, but it is sustained during most of the systolic phase Figure 7.

Energy loss

The energy loss allows to estimate the valve performance over the entire cycle, considering both the losses during forward flow and closing regurgitation (Akins et al., 2008).

The energy loss, expressed in millijoules (mJ), was calculated by integrating the product of the flow rate and transvalvular pressure over the relevant flow interval (Azadani et al., 2009) using Equation (2):

$$\text{Energy loss} = 0.1333 * \int_{t_i}^{t_f} \Delta p \times Q \times dt \qquad (2)$$

where t_i and t_f are the time instants used for integration, and Δp and Q are the instantaneous transvalvular pressure (in mmHg) and flow rate (in ml/s) during the time interval, respectively.

For the forward energy loss, the integral was computed between the beginning (t_1) and the end of the systolic phase (t_3). For the closing energy loss the integration was performed in the interval between the end of systole (t_3), and the valve closure instant (t_4).

A direct comparison of the energy losses for all conditions is given in Table 4. Forward and closing energy loss values for the young healthy configuration were found to be 67.7 mJ and 36.9 mJ, respectively.

Table 4. Energy loss values for healthy and aged configurations.

Configuration	Forward energy loss [mJ]	Closing energy loss [mJ]	Total energy loss [mJ]
Young healthy	67.7	36.9	104.6
Stiffened/Thickened tissues	107.78 (+59.2%)	108.92 (+195.17%)	216.7 (+107.17%)
Dilated root	51.77 (-23.53%)	72.16 (+95.5%)	123.93 (+18.4%)
Stiffened/Thickened tissues and dilated root	85.87 (+26.83%)	103.99 (+181.81%)	189.86 (+81.51%)

Discussion

This computational study provides a first thorough overview of the haemodynamic changes to be expected during the normal aging process, such as tissues stiffening and thickening, and progressive aortic root dilation. These have shown to substantially alter the haemodynamics and hydrodynamic efficiency of the aortic valve.

The most significant variations in terms of valvular kinematics are observed during closure (longer VCT). In fact, whilst the biggest percentage difference in terms of VOT with respect to the young healthy valve case is observed for the model with stiffened/thickened tissues in a dilated aortic root, and is 40%, the difference in VCT for the same model rises up to 160% (Table 2). The models with stiffened tissues were the first to initiate opening, immediately followed by the model mimicking the progressive dilation of the root chamber, which, instead, was synchronised with the young healthy valve. This is justified by the fact that the leaflets were designed at rest (without an applied pressure difference) in a semi-open

configuration, as described in Tango *et al.* (Tango et al., 2018). This is consistent with observations on explanted human valves, which typically show a partially open configuration (Cheng et al., 2017; Schoen, 2008). Hence, they tend to recover the partially-open stress-free configuration as soon as the diastolic pressure becomes insufficient to force them into their fully closed position. Similarly, once they reach the stress-free configuration, they resist a further expansion to a fully open state, so that full opening is achieved later than for softer tissue cases. Similar behaviour is observed during the closing stage when higher pressures are required to force the leaflets to move from the semi-open design configuration to complete coaption. This is consistent with the change of slope observed for the two stiffened models in the diagrams of the radial displacement (Figure 4) during the closing phase.

The simulations confirm that the primary function of the Sinuses of Valsalva is to host the open leaflets, in order to reduce their interference with the central jet (Tango et al., 2018). In fact, vortical structures into the sinuses are evident only at the distal region, and do not appear to play a role during the systolic phase. This mechanism was observed in all models analysed in this study.

Globally, the energy loss variations with respect to the young healthy case were found to be +107.17% for the stiffened valve configuration, +18.4% for the model with the dilated aorta, and +81.51% for the analysis with stiff leaflets and dilated root. Therefore, mild stiffening affects to a greater extent the haemodynamics and valve performance of the ascending aorta than those exhibited by dilated aortic root configurations. Larger root chamber improved the system energy efficiency in the opening phase, when the material properties are kept unchanged, with a trade off during the closing phase. In fact, the dilated model with unchanged stiffness presented the lowest forward energy loss values, consistently with a larger EOA and lower systolic Δp. However, this improvement is completely cancelled during closing, when the energy loss is almost double than that of the young healthy configuration (+95.5%), due to the longer time it takes to complete closure, which makes the valve less effective in containing the closing leakage. As a result, the valve performance over the full cardiac cycle was worse than for the healthy young model, with an increase in the total energy loss of nearly 20%. It does not come as a surprise that the configuration representing more closely the proportions adopted by nature in young subjects is confirmed to be the most efficient (Sirois et al., 2011; Swanson and Clark, 1974). However, it needs to be considered

that the model with the expanded aortic root, where the leaflets are proportionally extended in order to achieve full and complete coaption, is based on a favourable assumption. In fact the aortic root's growth often results in aortic regurgitation (Otto, 2000), suggesting that the leaflets' remodelling may not accommodate the root expansion, resulting in worse performance in terms of EOA and closing leakages, compared to those estimated in the presented study.

However, it is interesting that our study suggests that its optimum performance is the result of a compromise between the systolic performance, which could still be improved by enlarging the aortic root, and the closing performance, which worsens for larger valve dimensions. Also, this analysis supports the use of the concept of energy loss to achieve a meaningful characterisation of heart valves performances, rather than independently analysing the EOA and the regurgitant fraction, which is the current standard.

The results suggest that even low degrees of tissue stiffening strongly affect the valve function. Aortic root dilation, which per se results in lower efficiency during the whole cardiac cycle, can though contribute to mitigate the impairment due to the altered mechanical properties by enlarging the available flow areas.

This study provides a haemodynamic baseline associated with the physiological ageing process which allows to discriminate between normal ageing and pathological conditions.

The analysis of the shear stress was not included as it did not indicate significant variations between the different models. Overall, peaks of shear stress magnitude were around 10 MPa, well below the hemolytic threshold, which is reported to range from 20 to 500 Pa, depending on the source.

Limitations

The limitations of this work are mainly related to the geometry idealisation adopted for the valve and root (Thubrikar, 1990). The leaflets were assumed to behave as homogenous isotropic membranes disregarding their highly anisotropic layered structure and the variations of thickness in the various regions (such as the lunule and the nodulus of Arantius).

The viscoelastic nature of the tissues, which may have some effect on the quantified energy loss, was not modelled.

In reality, native aortic valve and aortic root geometrical shape and dimensions are strongly dependent upon the dimensions and size within each individual, presenting relevant degrees of asymmetry. The physiology of the native aorta is longer and more complex than that presented in this study, which could induce alterations to the fluid dynamics.

Blood behaviour was modelled as Newtonian, and the presence of coronary arteries was not included in the investigated models and requires further study.

Acknowledgements

This work was supported by the Rosetrees Trust (Grant Ref. A730) and supporting benefactors.

Conflict of interest

The authors declare that they have no conflict of interest.

References

Akins, C.W., Travis, B., Yoganathan, A.P., 2008. Energy loss for evaluating heart valve performance. J. Thorac. Cardiovasc. Surg. 136, 820–33. https://doi.org/10.1016/j.jtcvs.2007.12.059

Amindari, A., Saltik, L., Kirkkopru, K., Yacoub, M., Yalcin, H.C., 2017. Assessment of calcified aortic valve leaflet deformations and blood flow dynamics using fluid structure interaction modeling. Informatics Med. Unlocked 9, 191–199. https://doi.org/10.1016/j.imu.2017.09.001

Annio, G., Torii, R., Ariff, B., O'Regan, D.P., Muthurangu, V., Ducci, A., Tsang, V., Burriesci, G., 2019. Enhancing magnetic resonance imaging with computational fluid dynamics. J. Eng. Sci. Med. Diagnostics Ther. 2, 1–11. https://doi.org/10.1115/1.4045493

Azadani, A.N., Jaussaud, N., Matthews, P.B., Ge, L., Guy, T.S., Chuter, T.A.M., Tseng, E.E., 2009. Energy loss due to paravalvular leak with transcatheter aortic valve implantation. Ann. Thorac. Surg. 88, 1857–1863. https://doi.org/10.1016/j.athoracsur.2009.08.025

Bäck, M., Gasser, T.C., Michel, J.-B., Caligiuri, G., 2013. Biomechanical factors in the biology

of aortic wall and aortic valve diseases. Cardiovasc. Res. 99, 232–241. https://doi.org/10.1093/cvr/cvt040

Barannyk, O., Oshkai, P., 2015. The Iifluence of the aortic root geometry on flow characteristics of a prosthetic heart valve. J. Biomech. Eng. 137, 051005. https://doi.org/10.1115/1.4029747

Carmody, C.J., Burriesci, G., Howard, I.C., Patterson, E.A., 2006. An approach to the simulation of fluid-structure interaction in the aortic valve. J. Biomech. 39, 158–169. https://doi.org/10.1016/j.jbiomech.2004.10.038

Cheng, C.L., Chang, H.H., Huang, P.J., Wang, W.C., Lin, S.Y., 2017. Ex vivo assessment of valve thickness/calcification of patients with calcific aortic stenosis in relation to in vivo clinical outcomes. J. Mech. Behav. Biomed. Mater. 74, 324–332. https://doi.org/10.1016/j.jmbbm.2017.06.020

Craiem, D., Chironi, G., Redheuil, A., Casciaro, M., Mousseaux, E., Simon, A., Armentano, R.L., 2012. Aging impact on thoracic aorta 3D morphometry in intermediate-risk subjects: looking beyond coronary arteries with non-contrast cardiac CT. Ann. Biomed. Eng. 40, 1028–1038. https://doi.org/10.1007/s10439-011-0487-y

Crawford, M.H., Roldan, C.A., 2001. Prevalence of aortic root dilatation and small aortic roots in valvular aortic stenosis. Am. J. Cardiol. 87, 1311–1313. https://doi.org/10.1016/S0002-9149(01)01530-2

Guala, A., Camporeale, C., Ridolfi, L., 2015. Compensatory effect between aortic stiffening and remodelling during ageing. PLoS One 10, 1–14. https://doi.org/10.1371/journal.pone.0139211

Hallquist, J.O., 2006. LS-DYNA Theory Manual.

International Standard ISO 5840:2009, n.d. Cardiovascular implants - Cardiac valve prostheses (ISO 5840:2015).

Joda, A., Jin, Z., Haverich, A., Summers, J., Korossis, S., 2016. Multiphysics simulation of the effect of leaflet thickness inhomogeneity and material anisotropy on the stress–strain distribution on the aortic valve. J. Biomech. 49, 2502–2512.

https://doi.org/10.1016/j.jbiomech.2016.02.041

Kirali, K., Günay, D., 2017. Isolated Aortic Root Aneurysms, in: Aortic Aneurysm. InTech, p. 13. https://doi.org/10.5772/66963

Leyh, R.G., Schmidtke, C., Sievers, H.-H., Yacoub, M.H., 1999. Opening and closing characteristics of the aortic valve after different types of valve-preserving surgery. Circulation 100, 2153–2160. https://doi.org/10.1161/01.CIR.100.21.2153

M. Souli, A. Ouahsine, L.L., 2017. ALE formulation for fluid-structure interactions. Comput. Methods Appl. Mech. Eng. 118, 203–254. https://doi.org/10.1007/978-3-319-63970-3_5

Mao, S.S., Ahmadi, N., Shah, B., Beckmann, D., Chen, A., Ngo, L., Flores, F.R., Gao, Y. lin, Budoff, M.J., 2008. Normal thoracic aorta diameter on cardiac computed tomography in healthy asymptomatic adults. Acad. Radiol. 15, 827–834. https://doi.org/10.1016/j.acra.2008.02.001

Marom, G., 2015. Numerical Methods for Fluid–Structure Interaction Models of Aortic Valves. Arch. Comput. Methods Eng. 22, 595–620. https://doi.org/10.1007/s11831-014-9133-9

Marom, G., Halevi, R., Haj-Ali, R., Rosenfeld, M., Schäfers, H.J., Raanani, E., 2013. Numerical model of the aortic root and valve: Optimization of graft size and sinotubular junction to annulus ratio. J. Thorac. Cardiovasc. Surg. 146, 1227–1231. https://doi.org/10.1016/j.jtcvs.2013.01.030

Martin, C., Sun, W., Primiano, C., McKay, R., Elefteriades, J., 2013. Age-dependent ascending aorta mechanics assessed through Multiphase CT. Ann. Biomed. Eng. 41, 2565–2574. https://doi.org/10.1007/s10439-013-0856-9

Nobari, S., Mongrain, R., Gaillard, E., Leask, R., Cartier, R., 2012. Therapeutic vascular compliance change may cause significant variation in coronary perfusion: A numerical study. Comput. Math. Methods Med. 2012. https://doi.org/10.1155/2012/791686

Nobari, S., Mongrain, R., Leask, R., Cartier, R., 2013. The effect of aortic wall and aortic leaflet stiffening on coronary hemodynamic: A fluid-structure interaction study. Med.

Biol. Eng. Comput. 51, 923–936. https://doi.org/10.1007/s11517-013-1066-1

Otto, C.M., 2000. Aortic Stenosis — Listen to the patient, Look at the valve. N. Engl. J. Med. 343, 652–654. https://doi.org/10.1056/NEJM200008313430910

Querzoli, G., Fortini, S., Espa, S., Costantini, M., Sorgini, F., 2014. Fluid dynamics of aortic root dilation in Marfan syndrome. J. Biomech. 47, 3120–3128. https://doi.org/10.1016/j.jbiomech.2014.06.025

Ranga, A., Bouchot, O., Mongrain, R., Ugolini, P., Cartier, R., 2006. Computational simulations of the aortic valve validated by imaging data: evaluation of valve-sparing techniques. Interact. Cardiovasc. Thorac. Surg. 5, 373–378. https://doi.org/10.1510/icvts.2005.121483

Roman, M.J., Devereux, R.B., Niles, N.W., Hochreiter, C., Kligfield, P., Sato, N., Spitzer, M.C., Borer, J.S., 1987. Aortic root dilatation as a cause of isolated, severe aortic regurgitation. Prevalence, clinical and echocardiographic patterns, and relation to left ventricular. Ann. Intern. Med. 106, 800–807. https://doi.org/10.7326/0003-4819-106-6-800

Rossvoll, O., Samstad, S., Torp, H.G., Linker, D.T., Skjærpe, T., Angelsen, B.A.J., Hatle, L., 1991. The velocity distribution in the aortic Anulus in normal subjects: a quantitative analysis of two-dimensional Doppler flow maps. J. Am. Soc. Echocardiogr. 4, 367–378. https://doi.org/10.1016/S0894-7317(14)80447-1

Sacks, M.S., David Merryman, W., Schmidt, D.E., 2009. On the biomechanics of heart valve function. J. Biomech. 42, 1804–1824. https://doi.org/10.1016/j.jbiomech.2009.05.015

Sahasakul, Y., Edwards, W.D., Naessens, J.M., Tajik, A.J., 1988. Age-related changes in aortic and mitral valve thickness: Implications for two-dimensional echocardiography based on an autopsy study of 200 normal human hearts. Am. J. Cardiol. 62, 424–430. https://doi.org/10.1016/0002-9149(88)90971-X

Schoen, F.J., 2008. Evolving concepts of cardiac valve dynamics: The continuum of development, functional structure, pathobiology, and tissue engineering. Circulation 118, 1864–1880. https://doi.org/10.1161/CIRCULATIONAHA.108.805911

Seki, A., Fishbein, M.C., 2016. Age-related cardiovascular changes and diseases, in: Cardiovascular Pathology. Elsevier, pp. 57–83. https://doi.org/10.1016/B978-0-12-420219-1.00002-1

Sirois, E., 2014. Hemodynamic impact of transcatheter aortic valve deployment configuration 7, 2013–2014. https://doi.org/10.1115/1.4025938

Sirois, E., Wang, Q., Sun, W., 2011. Fluid simulation of a transcatheter aortic valve deployment into a patient-specific aortic root. Cardiovasc. Eng. Technol. 2, 186–195. https://doi.org/10.1007/s13239-011-0037-7

Sturla, F., Votta, E., Stevanella, M., Conti, C.A., Redaelli, A., 2013. Impact of modeling fluid-structure interaction in the computational analysis of aortic root biomechanics. Med. Eng. Phys. 35, 1721–1730. https://doi.org/10.1016/j.medengphy.2013.07.015

Sugawara, J., Hayashi, K., Yokoi, T., Tanaka, H., 2008. Age-associated elongation of the ascending aorta in Adults. JACC Cardiovasc. Imaging 1, 739–748. https://doi.org/10.1016/j.jcmg.2008.06.010

Swanson, W.M., Clark, R.E., 1974. Dimensions and geometric relationships of the human aortic value as a function of pressure. Circ. Res. 35, 871–882. https://doi.org/10.1161/01.RES.35.6.871

Tamburino,C.,Ussia, G.P., 2012. Percutaneous treatment of left side cardiac valves: a practical guide for the interventional cardiologist. Springer Science & Business Media,.

Tango, A.M., Salmonsmith, J., Ducci, A., Burriesci, G., 2018. Validation and extension of a fluid–structure interaction model of the healthy aortic valve. Cardiovasc. Eng. Technol. 9, 739–751. https://doi.org/10.1007/s13239-018-00391-1

Thubrikar, M.J., 1990. The aortic valve, 1st ed. ed. CRC Press, Boca Raton, FL.

Thubrikar, M.J., Labrosse, M.R., Zehr, K.J., Robicsek, F., Gong, G.G., Fowler, B.L., 2005. Aortic root dilatation may alter the dimensions of the valve leaflets. Eur. J. Cardio-thoracic Surg. 28, 850–855. https://doi.org/10.1016/j.ejcts.2005.09.012

Toninato, R., Salmon, J., Susin, F.M., Ducci, A., Burriesci, G., 2016. Physiological vortices in the sinuses of Valsalva: An in vitro approach for bio-prosthetic valves. J. Biomech. 49,

2635–2643. https://doi.org/10.1016/j.jbiomech.2016.05.027

Virmani, R., Avolio, A.P., Mergner, W.J., Robinowitz, M., Herderick, E.E., Cornhill, J.F., Guo, S.Y., Liu, T.H., Ou, D.Y., O'Rourke, M., 1991. Effect of aging on aortic morphology in populations with high and low prevalence of hypertension and atherosclerosis: Comparison between occidental and Chinese communities. Am. J. Pathol. 139, 1119–1129.

Vriz, O., Aboyans, V., D'Andrea, A., Ferrara, F., Acri, E., Limongelli, G., Della Corte, A., Driussi, C., Bettio, M., Pluchinotta, F.R., Citro, R., Russo, M.G., Isselbacher, E., Bossone, E., 2014. Normal values of aortic root dimensions in healthy adults. Am. J. Cardiol. 114, 921–927. https://doi.org/10.1016/j.amjcard.2014.06.028

Wei, Z.A., Sonntag, S.J., Toma, M., Singh-Gryzbon, S., Sun, W., 2018. Computational fluid dynamics assessment associated with transcatheter heart valve prostheses: a position paper of the ISO working group. Cardiovasc. Eng. Technol. https://doi.org/10.1007/s13239-018-0349-y

Wendt, D., Stühle, S., Marx, P., Benedik, J., Wendt, H., Stühle, T., Thoenes, M., Thielmann, M., Jakob, H., Kowalczyk, W., 2015. The investigation of systolic and diastolic leaflet kinematics of bioprostheses with a new in-vitro test method. Minim. Invasive Ther. Allied Technol. 24, 274–281. https://doi.org/10.3109/13645706.2015.1078818

Wilton, E., Jahangiri, M., 2006. Post-stenotic aortic dilatation. J. Cardiothorac. Surg. 1, 1–11. https://doi.org/10.1186/1749-8090-1-7

Yoganathan, A.P., 1988. Fluid mechanics of aortic stenosis. Eur. Heart J. 9, 13–17. https://doi.org/10.1093/eurheartj/9.suppl_E.13

Zhang, R., Zhang, Y., 2018. An experimental study of pulsatile flow in a compliant aortic root model under varied cardiac outputs. Fluids 3, 71. https://doi.org/10.3390/fluids3040071

Zhang, W., Chen, H.Y., Kassab, G.S., 2007. A rate-insensitive linear viscoelastic model for soft tissues. Biomaterials 28, 3579–3586. https://doi.org/10.1016/j.biomaterials.2007.04.040